The American Journal of Pathology, Vol. 175, No. 4, October 2009

DOI: 10.2353/ajpath.2009.090372

Neurobiology

Degenerating Synaptic Boutons in Prion Disease

Microglia Activation without Synaptic Stripping

Zuzana Šišková,* Anton Page,†
Vincent O'Connor,* and Victor Hugh Perry*

From the CNS Inflammation Group, School of Biological Sciences, and the Biomedical Imaging Unit,† School of Medicine, University of Southampton, Southampton, United Kingdom*

A growing body of evidence suggests that the loss of synapses is an early and major component of a number of neurodegenerative diseases. Murine prion disease offers a tractable preparation in which to study synaptic loss in a chronic neurodegenerative disease and to explore the underlying mechanisms. We have previously shown that synaptic loss in the hippocampus underpins the first behavioral changes and that there is a selective loss of presynaptic elements. The microglia have an activated morphology at this stage but they have an anti-inflammatory phenotype. We reasoned that the microglia might be involved in synaptic stripping, removing synapses undergoing a degenerative process, and that this gives rise to the anti-inflammatory phenotype. Analysis of synaptic density revealed a progressive loss from 12 weeks post disease initiation. The loss of synapses was not associated with microglia processes; instead, we found that the postsynaptic density of the dendritic spine was progressively wrapped around the degenerating presynaptic element with loss of subcellular components. Three-dimensional reconstructions of these structures from Dual Beam electron microscopy support the conclusion that the synaptic loss in prion disease is a neuron autonomous event facilitated without direct involvement of glial cells. Previous studies described synapse engulfment by developing and injured neurons, and we suggest that this mechanism may contribute to developmental and pathological changes in synapse numbers. ***(Am J Pathol 2009, 175:1610–1621; DOI: 10.2353/ajpath.2009.090372)***

A number of chronic progressive neurodegenerative diseases, such as Alzheimer's disease (AD) and prion disease (PD) are characterized by the accumulation of a misfolded protein that is deposited as amyloid in the extracellular space.[1] In AD the identification of the amyloid-β (Aß) peptide, derived from the amyloid precursor protein (APP) led to the amyloid cascade hypothesis. This hypothesis proposed that the Aß peptide triggers a cascade of molecular events that leads to the death of neurons in selected regions of the brain and ultimately to the development of cognitive impairments and behavioral dysfunction.[2] The identification of the prion protein PrP^{C}, and its misfolding to generate a protease-resistant form PrP^{Sc}, is similarly implicated in the demise of neurons in the chronic fatal neurodegenerative diseases known as the prion diseases.[3] Recent evidence suggests, however, that it is not the amyloid per se that is the neurotoxic element but it is oligomers of the Aß peptide[4] or misfolded PrP^{C} that may be critical in causing neuronal dysfunction and precipitating neurodegeneration.[5]

Whatever the nature of the toxic agent there is a growing body of data to show that it is the synapses that are the first or most susceptible component of the neuron to succumb in the disease process rather than the death of the cell soma.[6] In AD the loss of synapses correlates with the degree of dementia[7] and is an early component of the disease.[8] In murine prion disease the time of appearance of the earliest behavioral deficits is associated with a loss of synapses in the stratum radiatum of the hippocampus[9,10] before the detectable loss of neurons in CA1 or a detectable increase in apoptosis in other regions of the brain.[10] The dissociation between cell loss and synaptic loss is reinforced in prion models by studies showing that preventing neuronal degeneration does not prevent disease progression.[11,12]

Studies on the slow Wallerian degeneration mutant mouse (Wld^{s}) demonstrated for the first time that degeneration of the synapse and axon are active autodestruc-

Supported by UK Medical Research Council (MRC) grant G0501636.

Accepted for publication June 30, 2009.

Supplemental material for this article can be found on *http://ajp.amjpathol.org*.

Address reprint requests to Zuzana Šišková, M.Sc., Ph.D.; CNS Inflammation Group, Basset Crescent East, School of Biological Sciences, University of Southampton, SO16 7PX Southampton, UK. E-mail: z.siskova@soton.ac.uk.

tive processes, akin to programmed cell death, but differently regulated from death of the cell soma.[13,14] The loss of supernumerary synapses from the developing brain is well established and this may also involve tagging of the synapse by components of the complement cascade C1q and C3 for removal by microglia: it was suggested that a similar process might operate in glaucoma and by extension in other chronic neurodegenerative diseases.[15] Following peripheral nerve injury there is a rapid loss of synapses from the cell soma and dendrites of motor neurons and a number of authors have implicated microglia in the active removal of these afferent synapses, so called "synaptic stripping."[16,17] Associated with the spread of prion disease pathology the microglia adopt a typical activated morphology[18] but they have an anti-inflammatory mediator profile[19] that is typical of macrophages, which have digested apoptotic cells.[20] We thus set out to investigate features of synaptic degeneration in this model of chronic neurodegeneration to determine whether microglia are involved in synaptic stripping or phagocytosis of the degenerating synapses.

Materials and Methods

Animals

C57BL/6J (Harlan) female mice age 8 to 10 weeks were obtained from Harlan Laboratories (Bicester, UK) and were group-housed within the animal care facilities in Southampton University as described previously.[10]

Surgeries

All operations were performed under the UK Home Office license, as described previously.[10] Briefly, surgery was performed when these mice were 11 to 12 weeks old. Mice were anesthetized by intraperitoneal injection of Avertin (2,2,2-tribromoethanol solution) (20 ml/kg) and mounted in a stereotaxic frame (David Kopf Instruments, Tujunga, CA). Injections of 1 μl of homogenate (10% w/v in sterile PBS) of either normal C57 mouse brain (NBH-animals) or of a ME7 prion agent-infected brain (ME7-animals) were made bilaterally into the dorsal hippocampus with a 10-μl Hamilton syringe. The suspension was slowly infused and the needle was left in place for 2 minutes before being slowly withdrawn. Mice were placed in a heated recovery chamber and when fully recovered rehoused in groups and checked daily.

Tissue Preparation

NBH- and ME7-animals, in groups of three, were terminally anesthetized with sodium pentobarbital and euthanized by perfusion fixation for transmission electron microscopy at 10, 12, 16, and 18 weeks post injection (p.i.), to study the onset and progression of synaptic loss. A slow cardiac perfusion (20 to 30 minutes) was performed with fixative containing 3.4% paraformaldehyde, 1.25% glutaraldehyde, 0.2% picric acid in 0.1 M/L sodium phosphate buffer (final pH 7.2 to 7.4) immediately after short

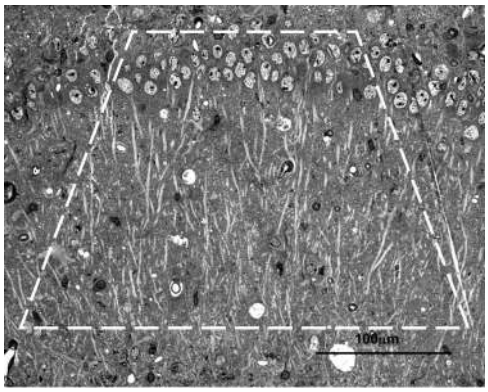

Figure 1. Light microscopic image illustrating sampling region from NBH-injected adult mouse hippocampus. Semithin (0.5-μm thick), toluidine blue stained section of a ME7-injected mouse hippocampus at 16 weeks p.i. Pyramidal cell bodies (upper part) and dendritic arbors in the stratum radiatum below are seen within a frame representing the area of an electron microscopic section. Scale bar = 100 μm.

(<1.5 minutes) perfusion with heparinized saline, to minimize synaptic and glial ultrastructural changes that could be caused by brain hypoxia.[21] After approximately 1 hour, the brains were dissected and postfixed in fresh fixative overnight at 4°C; 150 μm thick coronal sections were cut on a vibrotome and the area of CA1 pyramidal layer and stratum radiatum was dissected out. Microdissected areas were washed in 0.1 M/L sodium phosphate buffer and postfixed at room temperature for 1 hour in 1% osmium tetroxide. Tissue blocks were dehydrated at room temperature through graded ethanols from 30% to 100% for 10 minutes each, including 1% uranyl acetate in 70% ethanol for 40 minutes. Blocks were placed in acetonitrile for 10 minutes and overnight in a 50:50 solution of acetonitrile:TAAB resin, subsequently infiltrated with fresh TAAB resin for 6 hours and polymerized at 60°C for 20 to 24 hours. TAAB blocks were hand-trimmed, followed by glass trimming at room temperature to a trapezoid containing CA1 pyramidal cell bodies and dendritic arbor of stratum radiatum. Semithin (0.5 to 1 μm) sections were stained (1% v/v toluidine blue in 1% w/v borax) and used to guide further cutting of the specimen block into ultra-thin sections (60 to 70 nm) (Figure 1). Ultra-thin sections were placed onto either thin bar mesh copper palladium grids or formvar-coated slot grids or stained in Reynolds lead stain for 5 minutes. The grids were gently immersed three times in distilled water and then left to dry. Grids were examined using a Hitachi H7000 transmission electron microscope with a MegaView III digital camera (Soft Imaging System) and subsequently processed using Adobe Photoshop software (Adobe Systems Incorporated, San Jose, CA).

Electron Microscopy of Stratum Radiatum Synapses

Synapse Quantification

Synaptic profiles were analyzed on the basis of ultrastructural parameters and classified as type I (asymmetric) or type II (symmetric) synapses.[22] Synapses with

cross, obliquely or tangentially sectioned prominent asymmetric postsynaptic density (PSD) were considered as type I, if the PSD and cleft material were present on the reference section, and synaptic vesicles were present in the reference or immediately adjacent sections. Intact presynaptic terminals (containing visible synaptic vesicles) with a postsynaptic terminal in typical membrane apposition were included as synapses in the quantification study. For unbiased estimates of synaptic density, both NBH- and ME7-animals at 10, 12, 16, and 18 weeks p.i. were compared using the Disector method.[23] Disector pairs were collected from sections of uniform thickness at three different levels from the block face at least ten sections apart, to prevent overlapping (at magnification × 10,000). Disector pairs were positioned to avoid blood vessels, occasional areas of myelination and proximal fibril filled astrocytic processes that are present during prion–induced neurodegeneration.[10] A counting frame of 100 μm^2 overlying the disector pairs was selected; only intact synapses that were present in look-up sections and absent from the reference sections were counted and vice versa ($n = 6$ counts for animal at each time point per experimental group).

Measurements of PSD Areas and Presynaptic Terminal Areas

Measurements of PSD areas and presynaptic terminal areas were performed on asymmetric synapses at 10, 12, 16, and 18 weeks p.i. at a magnification × 20,000. The area of a PSD was measured only if synaptic vesicles were present in the same section and typical membrane apposition between presynaptic and postsynaptic element was present. At least 300 PSDs and 300 presynaptic terminals were measured for each time point from three different sections at least ten sections apart for both NBH- and ME7-animals (minimum $n = 100$ for animal/time point for each experimental group). The areas of presynaptic terminals containing synaptic vesicles and PSDs were included only if synaptic terminal profiles were clearly visible. Measurements of PSDs areas and presynaptic terminal areas were performed using outline spline function (by encircling and determining the area of individual objects) within the Axiovision (Carl Zeiss) and its equivalent within the ImageJ software (U.S. National Institutes of Health, *http://rsb.info.nih.gov/ij/download.html*). The identities of the coded images were only revealed to the observer after the data analysis was complete.

Measurement of PSD Curvature

The curvature of a PSD has been expressed as the angle of its arc above a chord drawn between its ends.[21] An angle of 180 deg denotes a flat PSD, which does not arc. PSDs that arch into the presynaptic terminals (convex) were given a negative value, however, these profiles were rarely detected. Those that arc into the dendritic spines (concave) were given a positive value. Measurement of PSD curvature was performed using Axiovision software, at least 300 PSDs (minimum $n = 100$ for animal/time point for each experimental group) were measured at magnification × 20,000 for both NBH- and ME7-animals at 10, 12, 16, and 18 weeks p.i. The identities of the coded images were only revealed to the observer after the data analysis was complete.

Serial Section Analysis

Images from serial sections through synaptic profiles involving degenerating terminals were prepared from 16 and 18 weeks p.i. ME7-animals using two different approaches with material prepared as above. Serial 70-nm sections were cut and collected on formvar coated slot grids, viewed, and photographed as described.

We also used the recently described Dual Beam system to generate serial sections for three-dimensional reconstructions.[24] Brain specimens were fixed and sectioned as for conventional transmission electron microscopy (see above). After locating a suitable area for analysis the blocks were trimmed to expose the side as well as the top of the tissue and the resin surrounding the tissue was heavily coated with silver dag (Agar Scientific, Stansted, UK) to reduce electrostatic charging. The sample was then placed in a carbon coater to further reduce charging on the sample surface. The blocks were then mounted in the specimen holder of an FEI Helios Dual Beam microscope (FEI Eindhoven, The Netherlands) and the tissue was located using electron backscatter imaging. A focused beam of gallium ions was used to cut two grooves alongside the tissue to help prevent sputtered material re-depositing back onto the surface to be imaged. The gallium beam was then used to remove vertical slices of tissue to expose a fresh block face. This block face was then imaged at 52 degrees by the electron beam again using backscatter imaging. Successive 28-nm slices were then removed from the block with a cut face approximately 40 μm wide by 40 μm high. After the ion beam removed each slice the resulting cut face was imaged by the electron beam. The slicing process was visually monitored for the first few cuts after which it was left for several hours or overnight to build up a data set of some 200 to 300-electron backscatter images. Since these images are of the tissue block rather than cut sections the data stack of images are in almost exact registration making the subsequent three-dimensional reconstruction more straightforward. A correction factor of 1.27 was applied to the y coordinates to compensate for the 52-degree tilt of the electron beam relative to the block face.

A custom program Reconstruct (*http://synapses.clm.utexas.edu*) was used for both conventional and Dual Beam material to align images from immediately adjacent serial sections and construct three-dimensional profiles.

Statistical Analysis

The identities of the coded blocks were only revealed to the observer after the data analysis was complete. Raw data from every block were collated using Microsoft Excel and two-tailed, unpaired Student's *t*-tests (PSD areas,

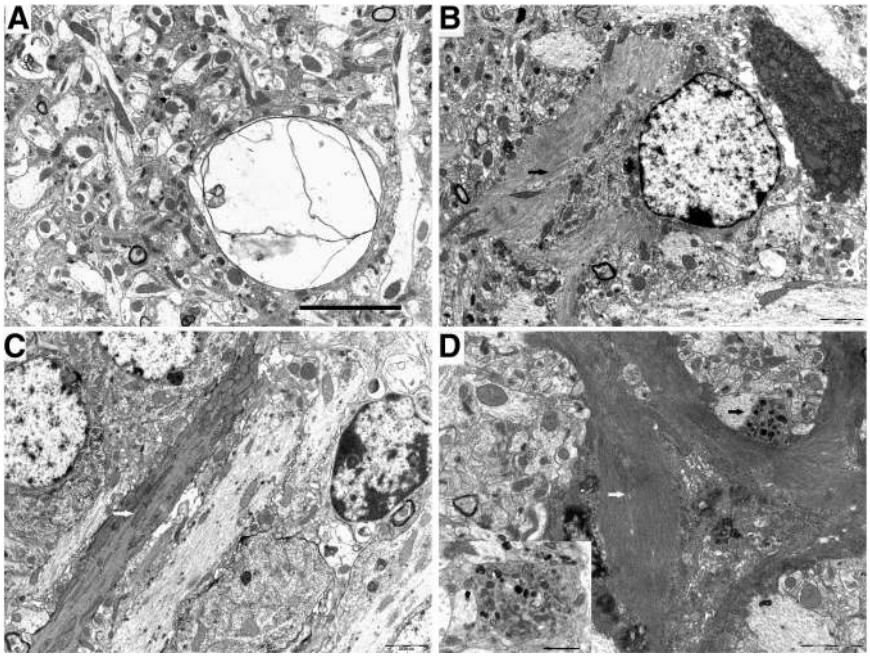

Figure 2. Electron micrographs of stratum radiatum of the hippocampus illustrating typical neuropathological hallmarks of prion disease. **A:** A characteristic spongiform vacuole within the hippocampal neuropil containing whorled membrane fragments. **B:** Astroglia with bundles of glial fibrils (**arrow**) from a ME7-animal at 16 weeks p.i. **C:** Electron opaque, degenerating dendrite at 18 weeks p.i. (**arrow**) was detected close to a cell showing chromatin condensation. **D:** Electron dense neuronal cytoplasm (**white arrow**), accumulation of neurofilament bundles was detected in neuronal somata (neuronal origin was confirmed by the presence of synaptic connections) at 18 weeks p.i. The neuropil contained membrane delimited profiles (**black arrow**, and **inset**) filled with secondary lysosomes. Scale bars: 5 μm (A); 2 μm (B); 2 μm (C); 2 μm (D); (**inset** 2 μm).

presynaptic terminal areas), respectively one-way analysis of variance with Tukey's multiple comparison tests (PSD curvature) were performed to compare final data between NBH ($n = 3$) and ME7-animals ($n = 3$) at each time point using GraphPad Prism software (GraphPad Software, Inc., CA).

The effect of the ME7 inoculation on synaptic density was compared with NBH at 10, 12, 16, and 18 weeks p.i., with three independent replicates in each of the eight samples. The synaptic density response was analyzed with fully-replicated and balanced two-way analysis of variance using the statistical model:

Response = Treatment + Time + Treatment*Time + ε

with two levels of Treatment (ME7 and NBH) and four levels of Time. Planned orthogonal contrasts were applied to the treatment-by-time interaction[25] to test for a contrast in the ME7 inoculation effect at 10 weeks against its average effect at 12 to 18 weeks, and for a change in effects between weeks 12 to 18 for type-I synaptic density, for type-II synaptic density planned orthogonal contrasts of week 18 to pooled weeks 10 to 16, and within weeks 10 to 16 were applied.

Results

The onset, incubation period and sequence of various pathological changes in murine ME7 scrapie have been previously described in a series of publications using different techniques.[26,27,28] Electron microscopy revealed the well-described ultrastructural hallmarks of the pathology in prion diseased brain[29] and these were present in all ME7-animals from 12 weeks p.i. onwards. Typical spongiform vacuoles developed within neuronal perikarya and processes[30,31] and were frequently detected in 16 and 18 weeks tissue in all ME7-animals and less frequently in 12 weeks tissue. Spongiform vacuoles in our material were always membrane-associated, occasionally with a double membrane, and frequently contained secondary vacuoles and whorling membrane fragments (Figure 2A). Numerous swollen astrocyte processes were present from 12 weeks p.i., surrounding the pyramidal cells in CA1 and at 16 and 18 weeks p.i., frequent astroglial processes with abundant filaments were detected in the stratum radiatum (Figure 2B; see Supplemental Figure S1 at *http://ajp.amjpathol.org*. for further description of ultrastructural criteria for the identification of astrocytes and neuronal cells). Subtle and gross neuronal abnormalities were detected almost exclusively in pyramidal cells, degenerating profiles were easily identified by a shrunken cell membrane plus a darkened cytoplasm with an apparent increase in mitochondrial density within neuritic processes, as well as darkened nucleoplasm and crenated nucleolemma within cell soma.

Prominent dendritic pathology was observed in ME7-animals at 18 weeks, numerous electron-dense, degenerating profiles were seen in the pyramidal CA1 layer and coursing across the stratum radiatum virtually devoid of synaptic connections on them (Figure 2C).

We did not find evidence of degenerating axons from CA3 pyramidal cells, which we would expect to be submicron in diameter, generally unmyelinated and forming *en passant* boutons on dendritic spines in the stratum radiatum. Evidence of degeneration of CA1 neurons with chromatin condensation, shrinking and darkening of neuronal cytoplasm was observed at 18 weeks: numerous membrane delimited profiles filled with secondary lysosomes were detected in cell bodies, dendrites and surrounding neuropil (Figure 2D). The dendritic alterations and loss of hippocampal pyramidal neurons have been documented in prion strains additional to ME7[32] and by different routes of challenge than intracerebral.[26] These

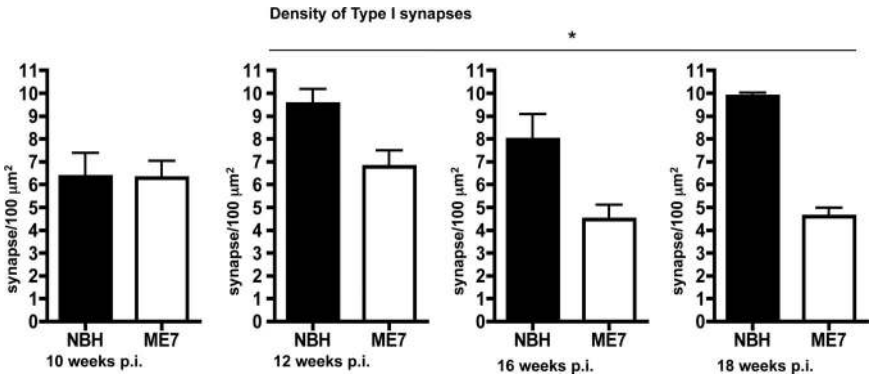

Figure 3. Density of type I synapses in stratum radiatum during prion disease progression. The density of type I synapses was determined using the disector method in aged-matched NBH-animals ($n = 3$) and ME7-animals ($n = 3$) animals at 10, 12, 16, and 18 weeks p.i. Data are presented as means ± SEM. An **asterisk** denotes statistical significance (see *Materials and Methods* for detailed description of the statistical analysis used). Note that type I synaptic density progressively decreased.

findings indicate that these features are common in prion diseases. In addition to these changes we observed changes in the appearance of presynaptic elements in the stratum radiatum, such as darkening of the presynaptic terminals that have previously been associated with synaptic degeneration. Therefore our next step was to investigate if any particular type of synapses was selectively involved during disease progression and to characterize this in further detail.

We analyzed synaptic density in NBH- and ME7-animals at 10, 12, 16, and 18 weeks p.i.. ME7 injection caused a reduction in the type-I synaptic density when compared with NBH (Figure 3, Table 1 $F_{1,16} = 29.84$, $P < 0.001$). The size of the effect treatment increased over time (Figure 3, Table 1 $F_{3,16} = 3.67$, $P = 0.035$), with a significant rise post-week 10 (Figure 3, Table 1 $F_{1,16} = 8.16$, $P = 0.011$).

At a relatively early time point (12 weeks p.i.), type I, glutamatergic synapses in the stratum radiatum of CA1 were reduced when compared with age-matched NBH-animals. No significant difference in type II synaptic density was detected at this stage between treated groups (Supplemental Table S1 at *http://ajp.amjpathol.org.*). At 16 and 18 weeks p.i. type I synaptic loss had further progressed (Figure 3). For the type II synaptic density we found no detectable effect of ME7 inoculation when compared with NBH, though week 18 approaches significance ($F_{1,16} = 2.72$, $P = 0.119$; see Supplemental Table S1 at *http://ajp.amjpathol.org*.). Our findings are supported by earlier studies that initially documented synaptic loss not only in the ME7 but also in the 87 V strain[27] with early selective reduction of the asymmetric synaptic density (type I) starting approximately from 12 weeks p.i.[9]

Table 1. Statistical Analysis of Type-I Synaptic Density

Source	DF	SS	MS	*F*	*P*
Time	3	12.148	4.049	2.32	0.115
(*i*) wk 10 vs average {wks 12, 16, 18}	1	0.915	0.915	0.52	0.480
(*ii*) wks 12 vs. 16 vs. 18	2	11.233	5.617	3.21	0.067
Treatment	1	52.168	52.168	29.84	<0.001
Treatment*Time	3	19.256	6.419	3.67	0.035
(*i*) Treatment* (wk 10 vs average {wks 12, 16, 18})	1	14.265	14.265	8.16	0.011
(*ii*) Treatment* (wks 12 vs. 16 vs. 18)	2	4.991	2.495	1.43	0.269
Error	16	27.972	1.748		
Total	23	111.544			

Output of two-way ANOVA, with orthogonal contrasts (*i*) between week 10 and subsequent weeks and (*ii*) between weeks 12 to 18.
*Treatment by time interaction.

The loss of type I synapses was accompanied by clear-cut evidence of degenerative abnormalities in both pre- and postsynaptic elements. In the stratum radiatum of NBH-animals typical type I asymmetric synapses appeared as previously described[22] with the majority of these synapses on dendritic spines having either linear or slightly curved PSDs (Figure 4, A–D). In contrast, in tissue from 16 and 18 weeks ME7-animals many terminals undergoing various stages of synaptic degeneration could be identified. The presynaptic element showed the signs typically associated with synaptic degeneration namely loss of definition of the individual synaptic vesicles and darkening of the cytoplasm within the intact presynaptic membrane. However the PSDs that remained in contact with the degenerating presynaptic elements were now progressively curved around the presynaptic element with greater degrees of engulfment associated with more advanced degeneration of the presynaptic structures (Figure 5, A–D, Figure 6C and see Supplemental Figure S2 at *http://ajp.amjpathol.org*). Of particular note was that in the many hundreds of synapses examined in ME7-animals at no stage was there evidence of another process intruding into the synaptic cleft between the pre- and postsynaptic elements, as might be expected if microglia or any other cell was involved in so-called synaptic stripping. We also could find no evidence of non-neuronal processes encircling the pre-synaptic element as a whole.

To quantify the changes in synaptic morphology during disease progression we measured three synaptic parameters intimately linked to synaptic function. Several studies[33–35] have suggested that small changes in synaptic geometry are sufficient to alter their physiological properties: the area of the PSD has been reported to correlate reliably with overall size/strength of type I synapse[36] and with the volume of the associated dendritic spine.[37] Changes in spine morphology as well as reorganization of PSD can occur relatively quickly, these changes can be induced by synaptic activation and have also been associated with synaptic plasticity.[38,39] Thus areas of PSDs and presynaptic terminals were measured, as was the curvature of the PSDs at 10, 12, 16, and 18

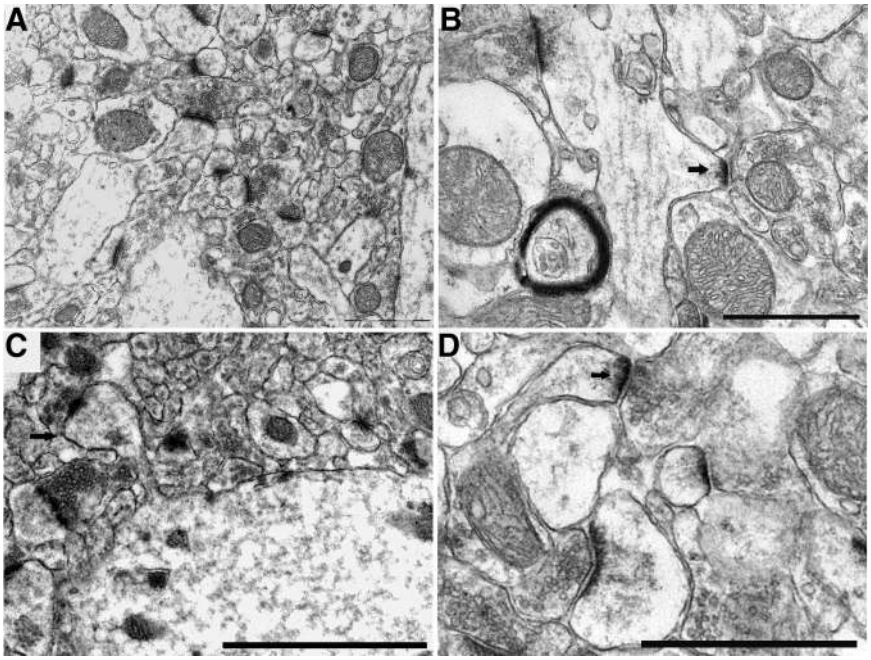

Figure 4. Electron micrographs showing intact synapses in NBH-animals at 16 **(A)** and 18 (**B–D**) weeks p.i. Presynaptic terminals are filled with electron-lucent cytoplasm, characteristic small round (<40 nm in diameter) synaptic vesicles and appose bar-like PSDs within an intact neuropil of the stratum radiatum without any signs of pathology or degeneration. Examples to illustrate the diversity of synaptic contacts are shown: a stubby spine (**B, arrow**) in which head width is equal to the neck length, a typical mushroom spine (**C, arrow**) with constricted neck and head exceeding 0.6 microns in diameter, and a thin spine (**D, arrow**) with characteristic thin neck and small head. Scale bars: 1 μm (**A, B, D**); 2 μm (**C**).

weeks p.i. and compared with age-matched controls. At 10 weeks, no detectable changes in the average area of PSDs or presynaptic terminals were observed (Table 2). However, at 12 weeks p.i., the areas of both post- and presynaptic elements were reduced in ME7-animals relative to NBH-animals (Figure 6, A–B; Table 2). From 12 weeks onwards the remaining PSDs gradually increased in size and at 18 weeks the mean area was bigger than those in age-matched NBH-animals at 18 weeks (Figure 6A; Table 2).

The curvature of the PSDs, described and illustrated below was quantified in 10, 12, 16, and 18 weeks NBH- and ME7-animals. A small numbers of synapses with highly curved PSDs were present at 12 weeks (Figure 6C), progressively increasing to significance at latter stages in ME7-animals (Figure 6D; Table 2). Virtually all of the PSDs in our study were concave with the degenerating presynaptic terminal remnant enveloped by the postsynaptic dendritic spine PSDs. No changes of curvature of the PSDs were detected in NBH-animals between 10 and 18 weeks postinjection.

The progressive curvature of spine PSDs observed in single 60 to 70 nm sections was highly suggestive of a process of engulfment or perhaps even internalization of the presynaptic element by the dendritic spine (Figure 7, A–D; see Supplemental Figure S3 at *http://ajp.amjpathol.org*). To investigate this further we performed detailed serial sec-

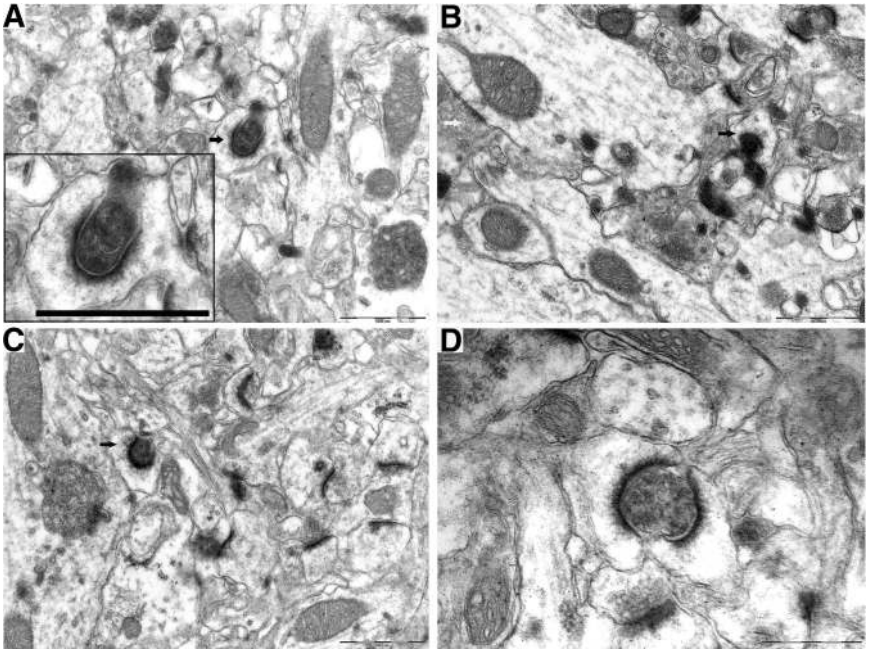

Figure 5. Type I synaptic junctions in stratum radiatum of animals with prion disease. Electron micrographs showing synaptic profiles with dramatically curved PSDs (**arrows**) at 16 (**A, B**) and 18 weeks (**C, D**) p.i. Some presynaptic terminals are shrunken and filled with electron-dense cytoplasm (**arrows**); others nearby appear normal. Some presynaptic vesicle-like structures are still apparent in degenerating terminals, which are apposed to dendritic spines with curved PSDs wrapping around the presynaptic element. Scale bars: 1 μm (**A–C**); 0.5 μm (**D**).

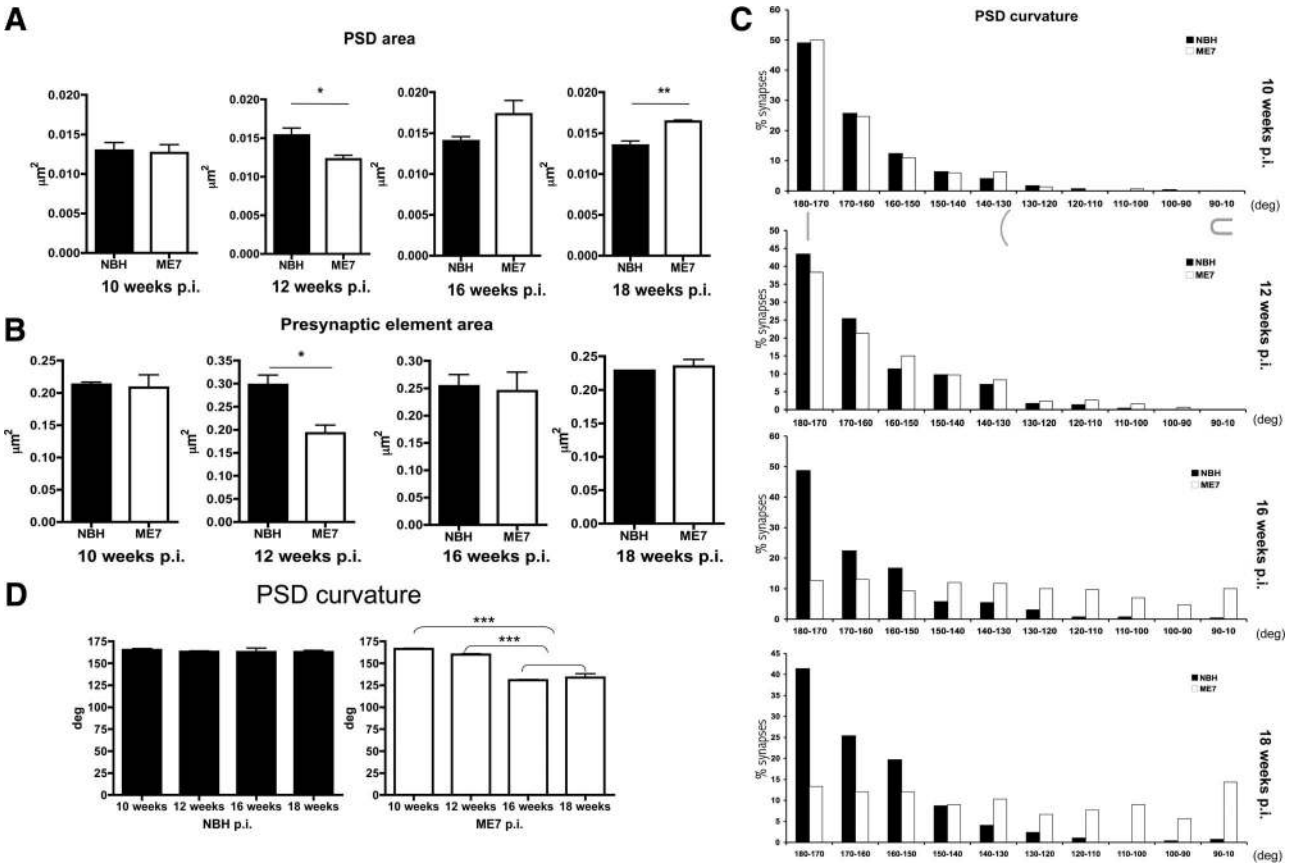

Figure 6. Quantification of structural changes of type I synaptic compartments across disease progression. The areas of PSDs (**A**) and presynaptic terminals (**B**) from either NBH-animals ($n = 3$) or ME7-animals ($n = 3$) show differential changes at different time points p.i. Data are presented as means ± s.e.m; two-tailed, unpaired Student's *t*-tests (*$P < 0.05$, ** $P < 0.01$). **C:** The curvature of the PSDs shows a progressive increase from 12 weeks onwards toward a more acute angle (the angle of its arc above a chord drawn between its ends, see *Material and Methods*). Note the appearance of groups of synapses with highly curved PSDs (<130 to 120 degrees) from 12 weeks onwards with a clear trend to significance in ME7-animals confirmed by one-way analysis of variance with Tukey's multiple comparison test ($P < 0.0001$). **D:** No changes of curvature were detected in NBH-animals from 10 to 18 weeks p.i. The PSD curvature data are also presented as means ± SEM in Table 2. Two-tailed, unpaired Student's *t*-tests (***$P < 0.001$).

tion analysis of 20 degenerating synaptic profiles. To facilitate the potential reconstruction of the relationship between the presynaptic element and dendritic spines we used Dual Beam imaging with serial 28-nm sections for increased precision. The image resolution from the Dual Beam microscope was comparable with that seen with conventional transmission electron microscopy. The reconstructions revealed evidence of almost, but not complete internalization of the presynaptic terminal by the PSD as shown by two representative profiles in Figure

Table 2. Quantification of Type I Synaptic Ultrastructural Changes at 10, 12, 16, and 18 Weeks in NBH- and ME7-Animals

	NBH mice	Prion-infected	*P* value (weeks post-injection)
PSD area (μm^2) mean ± SEM			
10	0.01293 ± 0.00101	0.01265 ± 0.00105	0.8452
12	0.01534 ± 0.00093	0.01224 ± 0.00051	0.0439*
16	0.01403 ± 0.00051	0.01733 ± 0.00164	0.1265
18	0.01350 ± 0.00051	0.01641 ± 0.00018	0.0058*
Presynaptic terminal area (μm^2) mean ± SEM			
10	0.2127 ± 0.003998	0.20800 ± 0.01985	0.8290
12	0.2970 ± 0.021140	0.19210 ± 0.01803	0.0195*
16	0.2536 ± 0.021220	0.24460 ± 0.03454	0.8350
18	0.2284 ± 0.000442	0.23480 ± 0.01046	0.5763
PSD curvature (deg) mean ± SEM			
10	165.4 ± 1.381	166.3 ± 0.5230	0.550
12	163.2 ± 0.981	159.9 ± 1.0070	0.078
16	162.8 ± 4.545	130.7 ± 0.5762	0.002*
18	162.8 ± 1.944	133.7 ± 4.5290	0.004*

Synaptic ultrastructural changes in NBH and ME7-infected mice.
*$P < 0.05$, two-tailed, unpaired Student's *t*-test, $n = 3$.

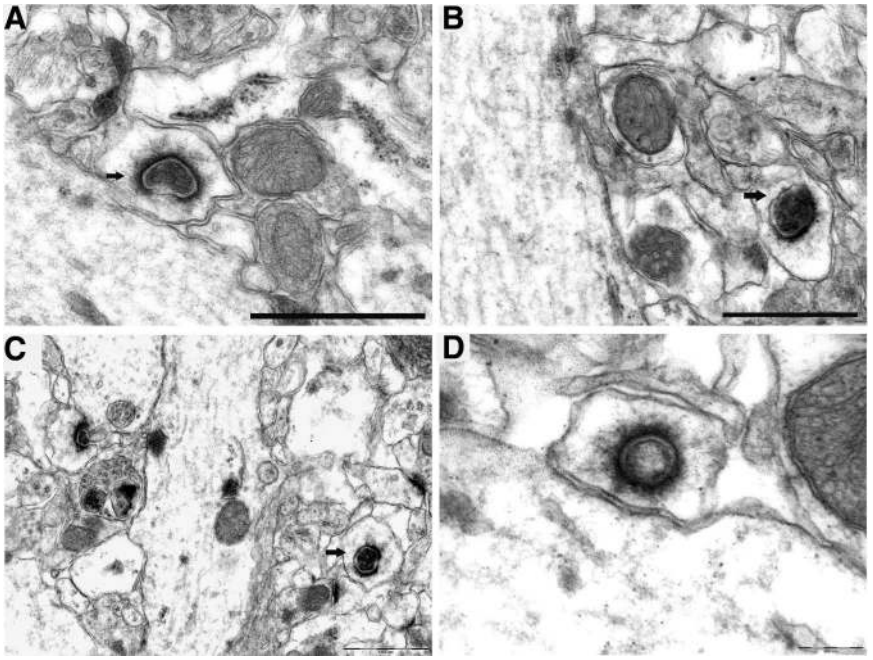

Figure 7. Degenerating type I presynaptic terminals in the stratum radiatum are enwrapped by dendritic spines during disease progression. Electron micrographs illustrating synaptic junctions at 16 (**A, B**) and 18 weeks (**C, D**) p.i. The presynaptic terminals of some synapses are collapsed and appear to be engulfed by the postsynaptic spine (**arrows**). Processes from other cell types were never observed in the synaptic cleft that involved degenerating presynaptic terminals. Scale bars: 1 μm (**A–C**); 0.2 μm (**D**).

8, A–B. The first 24 consecutive sections contributing to the profile in Figure 8A are illustrated in Figure 8C; the remaining 22 consecutive sections see Supplemental Figure S4 at *http://ajp.amjpathol.org*. The degenerating presynaptic element shows a dark cytoplasm with loss of definition of the vesicles but an intact presynaptic terminal membrane. The degenerated presynaptic element appeared to be collapsed and arrested on the PSD, separated from remaining retracted axon and open to the extracellular space. Microglia or astrocyte processes were never observed to be associated with these fragmented profiles. Despite extensive searching we did not observe fusion of the PSD with other organelles in the postsynaptic element, although we detected numerous autophagic vacuoles in the surrounding neuropil, which as described above increased with disease progression.

Discussion

We set out to investigate the possible role of microglia in the removal of synapses from the stratum radiatum during the progression of prion disease pathology. We detected an early decrease in the density of type I glutamatergic synapses from the stratum radiatum and this further increased as disease progressed. Associated with the decrease in density of glutamatergic synapses the remaining synapses hypertrophied. We also observed a progressive increase in the curvature of PSDs during disease progression and provided evidence that spine PSDs enwrap the degenerating presynaptic elements. Concomitant with this engulfment of the presynaptic terminals ultrastructural definition of presynaptic vesicles was progressively lost. The loss of these glutamatergic synapses did not involve any cell process other than the pre- and postsynaptic elements. Both microglia and astrocytes failed to directly participate in synapse removal or "synaptic stripping" during the evolution of ME7 induced prion pathology, or that induced by additional strains (Z. Siskova, V. O'Connor, and V.H. Perry, unpublished observations). However, we do not exclude that the possibility that microglia or astrocytes could participate indirectly by secreting molecules that may influence neuronal behavior.

We have investigated the synaptic density from 10 weeks after initiation of disease before any significant decline in expression of synaptic markers (synaptophysin),[10] to detect the first pathological changes in synaptic density and ultrastructure. In the stratum radiatum of the hippocampus the vast majority of glutamatergic synapses (approximately 90%) arise from axons of CA3 pyramidal neurons, which terminate on spines of proximal CA1 dendrites.[40] Consistent with the glutamatergic nature of this pathway virtually all synaptic terminals undergoing degeneration were in asymmetric contact with dendritic spines with characteristic, relatively small (<40 nm in diameter) round vesicles. Loss of these synapses has been linked to the first behavioral deficits in the absence of neuronal loss in CA1, the absence of cells positive for terminal deoxynucleotidyl transferase dUTP nick-end labeling in CA1 or CA3[10] or reduction in CA3 neuronal density.[41] An earlier electron microscopy study has described similar reduction of the asymmetric synaptic density taking place approximately at 80 days (about 12 weeks) p.i. in the stratum radiatum of CA1, these changes preceded the neuronal loss in CA1,[9] which is in agreement with our present study and previous findings.[10]

There is evidence that spine structure, including the dimensions of the PSD, are a crucial determinant of synaptic efficacy.[42,43] The first changes we detected were at 12 weeks p.i., when the area of the average type I synapse PSD in ME7-animals was smaller when compared

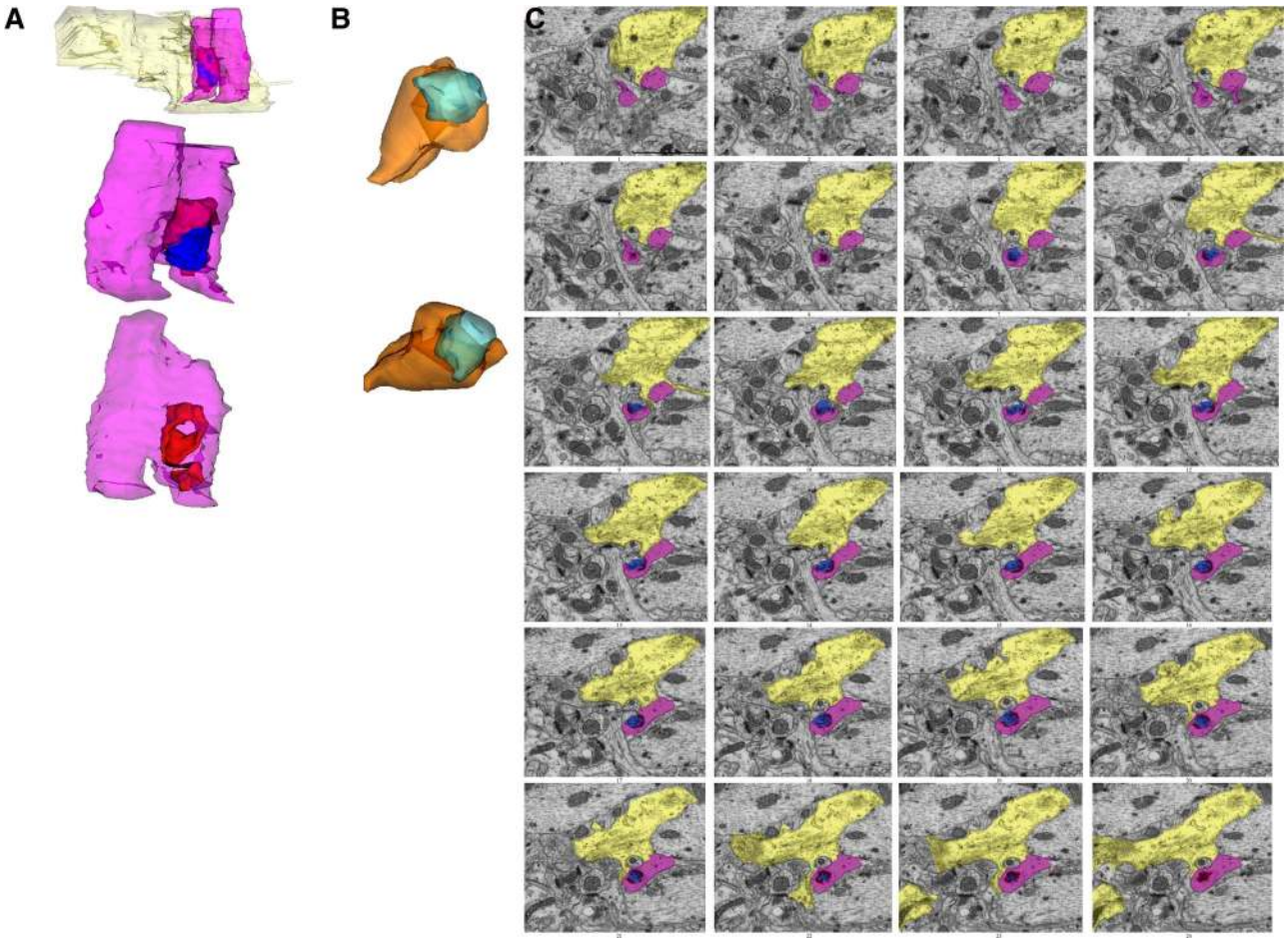

Figure 8. Computer-generated three-dimensional reconstructions of degenerating synapses in stratum radiatum of ME7-animals 18 weeks p.i. generated from serial Dual Beam microscope sections. **A:** Rotations of synaptic profile generated from 46 consecutive sections through individual degenerating synapse, material originating from presynaptic element (blue) remains both outside and inside (engulfed by the PSD [red]) of the dendritic spine (purple). Note the presence of astrocytic process (yellow) in close proximity but not engaged with the degenerating terminal. Sections from which the profile was generated are illustrated in Figure 8C (first 24 sections), for remaining sections see Supplemental Figure S3 at *http://ajp.amjpathol.org*. **B:** Rotations of a degenerating synaptic profile from 20 consecutive sections. Presynaptic element (blue) appears to be completely internalized by dendritic spine head (orange), serial sectioning confirmed however that a fine strand of material originating from presynaptic element remained in association with the extracellular space and was not within the encircling PSD of the spine. **C:** Electron micrographs of first 24 serial sections illustrating a degenerating synaptic terminal in the stratum radiatum of a ME7-animal at 18 weeks p.i. Presynaptic element (blue) cytoplasm remains electron-dense throughout all sections; although synaptic vesicles are still visible, the presynaptic element was disconnected from projecting axonal terminal, remained arrested and almost completely engulfed by PSD (red) of a dendritic spine (purple). An astrocytic cell process is in close proximity (yellow). Scale bar = 1 μm.

with NBH-animals and the average area of presynaptic terminals in these synapses was also reduced. This reduction in size of critical synaptic components at this stage, in addition to synaptic loss may underpin the early reduction in synaptic plasticity described in this model.[44] In addition to the early reduction in size of the presynaptic terminal our biochemical analysis has shown that proteins associated with synaptic vesicles are the first proteins to be down-regulated or degraded during disease progression.[41] At 18 weeks p.i., type I glutamatergic PSDs that remain, were significantly larger when compared with their age-matched NBH controls, perhaps indicative of a reactive hypertrophy. Synaptic loss is accompanied by synaptic hypertrophy in brains from Alzheimer's patients.[45,46]

A striking feature of the synaptic morphology during disease progression was the change in the curvature of the PSDs. An increase in PSD curvature and thickness has been shown to occur after a delay in transcardial perfusion fixation of the mouse brain, a condition that induces ischemic stress.[21] However, the PSDs in ischemic tissue arched into the presynaptic terminal to form convex PSDs, while in ME7-animals the PSDs were strikingly concave both at 16 and 18 weeks p.i.

The involvement of microglia in the removal of synapses was first suggested in the context of synaptic loss from facial motor neurons undergoing chromatolysis.[17] It was envisioned that the activated and proliferating microglia were actively involved in the removal of the synapses from the soma and proximal dendrites of the axotomised neurons. As the PSDs progressively enveloped the presynaptic element we did not observe the intrusion of processes into the synaptic cleft or around the presynaptic element. Furthermore, studies in which microglial proliferation was arrested by either pharmacological[47] or genetic[48] manipulations did not alter synaptic loss from neurons undergoing chromatolysis. At the present time it is unclear whether the microglia become activated as a

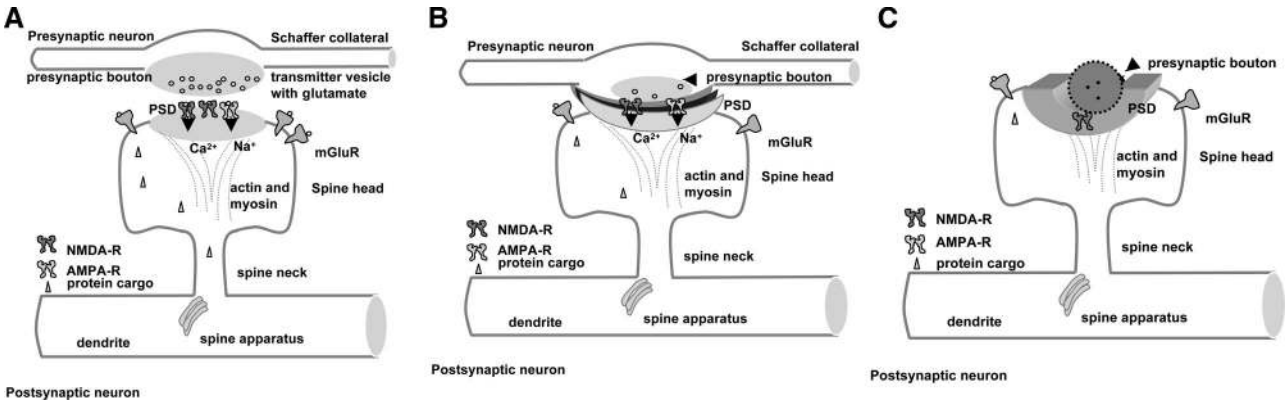

Figure 9. Presynaptic engulfment by postsynaptic dendritic spine in murine prion disease. **A:** A normal *en passant* bouton formed between a projecting CA3 Schaffer collateral axon and a dendritic spine of a CA1 pyramidal cell in stratum radiatum. Note the asymmetric PSD characteristic of type I synapses and molecular components within the PSD. **B:** As disease progresses, the vast majority of synapses in this region have curved PSDs that progressively wrap around the degenerating presynaptic element. **C:** At latter stages, the remnants of degenerating terminals appear completely engulfed by spine heads and disconnected from projecting terminals, but they remain connected to the extracellular space and are not completely internalized as evidenced by serial section reconstruction.

consequence of the accumulation of misfolded PrP^C or the initial synaptic alterations and what local signals lead to the expression of an anti-inflammatory phenotype.

As disease progressed we detected an increase in incidence of synaptic profiles in which the presynaptic element appeared to be completely internalized by the dendritic spine PSD. While single sections provided some evidence for the internalization of the presynaptic element it is only from serial sections that we can verify this observation. Conventional serial sections showed that the presynaptic element was almost entirely encircled by the PSD, but a fine strand of material still remained between the extracellular space and the residual presynaptic bouton. We have previously reported a selective loss of the presynaptic markers from affected axons that occurs relatively early on (about 12 weeks p.i.).[10,41] Of note is that the affected axons did not exhibit signs of degeneration, for example dark cytoplasm, suggesting that the degenerating presynaptic element was associated with the dendritic spine without the demise of the projecting axon that otherwise appeared unaltered. This finding is in agreement with our finding of early selective loss of proteins from the presynaptic compartment.[41] Reconstruction of serial sections from the Dual Beam microscope provided similar serial images of terminals completely enwrapped by the PSD. We searched for morphological evidence of what might be the next steps in the process but at present it is unclear what happens to the presynaptic element or the PSD. If this is a rapid process akin to the rapid degradation of a phagocytosed apoptotic cell this may require real-time imaging studies. Real-time imaging studies of dendritic spine loss during prion disease have shown that spine loss is associated with the development of varicosities on the dendritic shaft.[49] How the degeneration of the synapse, dendritic spine loss and the generation of dendritic varicosities are related remains to be resolved. However, at corresponding time points to the study described above, we detected numerous collapsed, darkened profiles that resembled shafts varicosities, which could precipitate dendritic pathology (see Supplemental Figure S5 at *http://ajp.amjpathol.org*).

There is evidence to demonstrate that neurons have a phagocytic capacity: the ingestion of diverse particulate matter has been described.[50] Phagocytosis of dying neurons by adjacent neuronal progenitors has been documented in the developing retina and spinal cord.[51–53] However, of particular interest are images showing that motor neurons in the developing spinal cord of the cat engulf supernumerary synapses on the motor neuron cell soma.[54] Similarly it has also been shown that injured hypoglossal motor neurons envelop synapses innervating the cell soma.[55] It is not clear from these studies what is the mechanism of recognition of the supernumerary synapses or the fate of the enveloped synapses. A recent study has proposed that during development supernumerary retinal ganglion cell synapses in the dorsal lateral geniculate nucleus are tagged by C1q and C3 synthesized by the retinal ganglion cells and subsequently removed by the microglia present in the vicinity.[15] However, as discussed previously,[56] and confirmed by earlier observations, the postsynaptic neuron itself may play a role in the regulation of synapse number in both development and chronic neurodegeneration.

The loss of dendritic spines and the degeneration of the presynaptic contact appear to be early components in various brain pathologies including prion disease.[49,57–59] Filamentous actin represents the major cytoskeletal component of dendritic spines[60] and changes in spine shape, size, and number are determined by local actin dynamics.[35,61] It is widely accepted that rapid remodeling of spines is determined by polymerization and depolymerization of actin filaments[62–64] and actin-dependent retraction of a dendritic spine can take place over a period as short as fifteen minutes; the spines were suggested to be more motile than presynaptic boutons.[65] Phagocytosis is defined as the cellular engulfment of large particles, usually over 0.5 μm in diameter and this too is known to be an actin-dependent process.[66] The process is also actin-dependent and extension of the plasma membrane around a particle is similar sequence to the morphological events we have described here. The mechanisms, be they pre- or postsynaptic that initiate this

intimate dynamic interaction between the degenerating pre-synaptic terminal and the PSD remain to be resolved.

We and others have previously shown that synaptic loss in this model of chronic neurodegeneration occurs before any neuronal loss.[9,10,41] In the present study we demonstrate that the synaptic degeneration does not involve microglia synaptic stripping but involves a PSD mediated engulfment of the presynaptic terminal (Figure 9, A–C). The linkage between the generation of PrP^{Sc} or oligomeric fibrils and the degeneration of synapses is not understood although we know that at 12 weeks p.i. PrP^{Sc} is sparsely distributed in the stratum radiatum.[10,67] Several studies have been performed in attempt to clarify the relationship between PrP^{Sc} accumulation and synaptic pathology.[27,68] The story is further complicated by the observation that neurons can exhibit prion-specific pathology despite lacking PrP^{C} expression in situation where the PrP^{C} expression in the brain is confined to astrocytes.[69] The molecular mechanisms that initiate and underlie the phagocytic-like behavior of the dendritic spine are a new dimension of synaptic pathology in chronic neurodegeneration and their background remains to be explored.

Acknowledgments

We thank Professor Peter Somogyi and David Roberts (MRC Neuroanatomical Pharmacology Unit, Oxford) for advice on electron microscopy; Richard Reynolds (School of Biological Sciences, Southampton) for technical support throughout; Dr. Hans Schuppe (School of Biological Sciences, Southampton) and personnel from Biomedical Imaging Unit (Southampton General Hospital) for helpful discussions and suggestions; and David Wall and Ben Lich (FEI company, Eindhoven, The Netherlands) for producing serial images using Dual Beam technology. We also thank Dr. Patrick Doncaster (School of Biological Sciences, Southampton) for help with statistical analysis.

References

1. Taylor JP, Hardy J, Fischbeck KH: Toxic proteins in neurodegenerative disease. Science 2002, 296:1991–1995
2. Hardy JA, Higgins GA: Alzheimer's disease: the amyloid cascade hypothesis. Science 1992, 256:184–185
3. Harris DA, True HL: New insights into prion structure and toxicity. Neuron 2006, 50:353–357
4. Selkoe DJ: Soluble oligomers of the amyloid beta-protein impair synaptic plasticity and behavior. Behav Brain Res 2008, 192:106–113
5. Caughey B, Baron GS: Prions and their partners in crime. Nature 2006, 443:803–810
6. Scheff SW, Price DA, Schmitt FA, Mufson EJ: Hippocampal synaptic loss in early Alzheimer's disease and mild cognitive impairment. Neurobiol Aging 2006, 27:1372–1384
7. Terry RD, Masliah E, Salmon DP, Butters N, DeTeresa R, Hill R, Hansen LA, Katzman R: Physical basis of cognitive alterations in Alzheimer's disease: synapse loss is the major correlate of cognitive impairment. Ann Neurol 1991, 30:572–580
8. Mesulam MM: Neuroplasticity failure in Alzheimer's disease: bridging the gap between plaques and tangles. Neuron 1999, 24:521–529
9. Jeffrey M, Halliday WG, Bell J, Johnston AR, MacLeod NK, Ingham C, Sayers AR, Brown DA, Fraser JR: Synapse loss associated with abnormal PrP precedes neuronal degeneration in the scrapie-infected murine hippocampus. Neuropathol Appl Neurobiol 2000, 26:41–54
10. Cunningham C, Deacon R, Wells H, Boche D, Waters S, Diniz CP, Scott H, Rawlins JN, Perry VH: Synaptic changes characterize early behavioural signs in the ME7 model of murine prion disease. Eur J Neurosci 2003, 17:2147–2155
11. Chiesa R, Piccardo P, Dossena S, Nowoslawski L, Roth KA, Ghetti B, Harris DA: Bax deletion prevents neuronal loss but not neurological symptoms in a transgenic model of inherited prion disease. Proc Natl Acad Sci USA: 2005, 102:238–243
12. Steele AD, King OD, Jackson WS, Hetz CA, Borkowski AW, Thielen P, Wollmann R, Lindquist S: Diminishing apoptosis by deletion of Bax or overexpression of Bcl-2 does not protect against infectious prion toxicity in vivo. J Neurosci 2007, 27:13022–13027
13. Lunn ER, Brown MC, Perry VH: The pattern of axonal degeneration in the peripheral nervous system varies with different types of lesion. Neuroscience 1990, 35:157–165
14. Mack TG, Reiner M, Beirowski B, Mi W, Emanuelli M, Wagner D, Thomson D, Gillingwater T, Court F, Conforti L, Fernando FS, Tarlton A, Andressen C, Addicks K, Magni G, Ribchester RR, Perry VH, Coleman MP: Wallerian degeneration of injured axons and synapses is delayed by a Ube4b/Nmnat chimeric gene. Nat Neurosci 2001, 4:1199–1206
15. Stevens B, Allen NJ, Vazquez LE, Howell GR, Christopherson KS, Nouri N, Micheva KD, Mehalow AK, Huberman AD, Stafford B, Sher A, Litke AM, Lambris JD, Smith SJ, John SW, Barres BA: The classical complement cascade mediates CNS synapse elimination. Cell 2007, 131:1164–1178
16. Blinzinger K, Kreutzberg G: Displacement of synaptic terminals from regenerating motoneurons by microglial cells. Z Zellforsch Mikrosk Anat 1968, 85:145–157
17. Moran LB, Graeber MB: The facial nerve axotomy model. Brain Res Brain Res Rev 2004, 44:154–178
18. Perry VH, Cunningham C, Holmes C: Systemic infections and inflammation affect chronic neurodegeneration. Nat Rev Immunol 2007, 7:161–167
19. Boche D, Cunningham C, Docagne F, Scott H, Perry VH: TGFbeta1 regulates the inflammatory response during chronic neurodegeneration. Neurobiol Dis 2006, 22:638–650
20. Fadok VA, Chimini G: The phagocytosis of apoptotic cells. Semin Immunol 2001, 13:365–372
21. Tao-Cheng JH, Gallant PE, Brightman MW, Dosemeci A, Reese TS: Structural changes at synapses after delayed perfusion fixation in different regions of the mouse brain. J Comp Neurol 2007, 501:731–740
22. Gray EG: Electron microscopy of synaptic contacts on dendrite spines of the cerebral cortex. Nature 1959, 183:1592–1593
23. Sterio DC: The unbiased estimation of number and sizes of arbitrary particles using the disector. J Microsc 1984, 134:127–136
24. Knott G, Marchman H, Wall D, Lich B: Serial section scanning electron microscopy of adult brain tissue using focused ion beam milling. J Neurosci 2008, 28:2959–2964
25. Doncaster CP, Davey AJH: Analysis of Variance: How to Choose and Construct Models for the Life Sciences. Cambridge, Cambridge University Press, 2007, pp. 245–247
26. Jeffrey M, Fraser JR, Halliday WG, Fowler N, Goodsir CM, Brown DA: Early unsuspected neuron and axon terminal loss in scrapie-infected mice revealed by morphometry and immunocytochemistry. Neuropathol Appl Neurobiol 1995, 21:41–49
27. Jeffrey M, Goodsir CM, Bruce ME, McBride PA, Fraser JR: In vivo toxicity of prion protein in murine scrapie: ultrastructural and immunogold studies. Neuropathol Appl Neurobiol 1997, 23:93–101
28. Jeffrey M, Martin S, Barr J, Chong A, Fraser JR: Onset of accumulation of PrPres in murine ME7 scrapie in relation to pathological and PrP immunohistochemical changes. J Comp Pathol 2001, 124:20–28
29. Jeffrey M, Goodbrand IA, Goodsir CM: Pathology of the transmissible spongiform encephalopathies with special emphasis on ultrastructure. Micron 1995, 26:277–298
30. Liberski PP: Spongiform change–an electron microscopic view, Folia Neuropathol 2004, 42 Suppl B:59–70
31. Jeffrey M, Scott JR, Williams A, Fraser H: Ultrastructural features of spongiform encephalopathy transmitted to mice from three species of bovidae. Acta Neuropathol 1992, 84:559–569
32. Belichenko PV, Brown D, Jeffrey M, Fraser JR: Dendritic and synaptic

alterations of hippocampal pyramidal neurones in scrapie-infected mice. Neuropathol Appl Neurobiol 2000, 26:143–149
33. Harris KM, Jensen FE, Tsao B: Three-dimensional structure of dendritic spines and synapses in rat hippocampus (CA1) at postnatal day 15 and adult ages: implications for the maturation of synaptic physiology and long-term potentiation. J Neurosci 1992, 12:2685–2705
34. Oertner TG, Matus A: Calcium regulation of actin dynamics in dendritic spines. Cell Calcium 2005, 37:477–482
35. Ryu J, Liu L, Wong TP, Wu DC, Burette A, Weinberg R, Wang YT, Sheng M: A critical role for myosin IIb in dendritic spine morphology and synaptic function. Neuron 2006, 49:175–182
36. Harris KM, Stevens JK: Dendritic spines of rat cerebellar Purkinje cells: serial electron microscopy with reference to their biophysical characteristics. J Neurosci 1988, 8:4455–4469
37. Harris KM, Stevens JK: Dendritic spines of CA 1 pyramidal cells in the rat hippocampus: serial electron microscopy with reference to their biophysical characteristics. J Neurosci 1989, 9:2982–2997
38. Toni N, Buchs PA, Nikonenko I, Povilaitite P, Parisi L, Muller D: Remodeling of synaptic membranes after induction of long-term potentiation. J Neurosci 2001, 21:6245–6251
39. Nikonenko I, Jourdain P, Alberi S, Toni N, Muller D: Activity-induced changes of spine morphology. Hippocampus 2002, 12:585–591
40. Steward O: Topographic organization of the projections from the entorhinal area to the hippocampal formation of the rat. J Comp Neurol 1976, 167:285–314
41. Gray BC, Siskova Z, Perry VH, O'Connor V: Selective presynaptic degeneration in the synaptopathy associated with ME7-induced hippocampal pathology. Neurobiol Dis 2009, 35:63–74
42. Naisbitt S, Valtschanoff J, Allison DW, Sala C, Kim E, Craig AM, Weinberg RJ, Sheng M: Interaction of the postsynaptic density-95/guanylate kinase domain-associated protein complex with a light chain of myosin-V and dynein. J Neurosci 2000, 20:4524–4534
43. Hung AY, Futai K, Sala C, Valtschanoff JG, Ryu J, Woodworth MA, Kidd FL, Sung CC, Miyakawa T, Bear MF, Weinberg RJ, Sheng M: Smaller dendritic spines, weaker synaptic transmission, but enhanced spatial learning in mice lacking Shank1. J Neurosci 2008, 28:1697–1708
44. Chiti Z, Knutsen OM, Betmouni S, Greene JR: An integrated, temporal study of the behavioural, electrophysiological and neuropathological consequences of murine prion disease. Neurobiol Dis 2006, 22:363–373
45. Bertoni-Freddari C, Fattoretti P, Casoli T, Meier-Ruge W, Ulrich J: Morphological adaptive response of the synaptic junctional zones in the human dentate gyrus during aging and Alzheimer's disease. Brain Res 1990, 517:69–75
46. DeKosky ST, Scheff SW: Synapse loss in frontal cortex biopsies in Alzheimer's disease: correlation with cognitive severity. Ann Neurol 1990, 27:457–464
47. Svensson M, Aldskogius H: Synaptic density of axotomized hypoglossal motorneurons following pharmacological blockade of the microglial cell proliferation. Exp Neurol 1993, 120:123–131
48. Kalla R, Liu Z, Xu S, Koppius A, Imai Y, Kloss CU, Kohsaka S, Gschwendtner A, Moller JC, Werner A, Raivich G: Microglia and the early phase of immune surveillance in the axotomized facial motor nucleus: impaired microglial activation and lymphocyte recruitment but no effect on neuronal survival or axonal regeneration in macrophage-colony stimulating factor-deficient mice. J Comp Neurol 2001, 436:182–201
49. Fuhrmann M, Mitteregger G, Kretzschmar H, Herms J: Dendritic pathology in prion disease starts at the synaptic spine. J Neurosci 2007, 27:6224–6233
50. Bowen S, Ateh DD, Deinhardt K, Bird MM, Price KM, Baker CS, Robson JC, Swash M, Shamsuddin W, Kawar S, El-Tawil T, Roos J, Hoyle A, Nickols CD, Knowles CH, Pullen AH, Luthert PJ, Weller RO, Hafezparast M, Franklin RJ, Revesz T, King RH, Berninghausen O, Fisher EM, Schiavo G, Martin JE: The phagocytic capacity of neurones. Eur J Neurosci 2007, 25:2947–2955
51. Garcia-Porrero JA, Ojeda JL: Cell death and phagocytosis in the neuroepithelium of the developing retina. A TEM and SEM study. Experientia 1979, 35:375–376
52. Homma S, Yaginuma H, Oppenheim RW: Programmed cell death during the earliest stages of spinal cord development in the chick embryo: a possible means of early phenotypic selection. J Comp Neurol 1994, 345:377–395
53. Yaginuma H, Tomita M, Takashita N, McKay SE, Cardwell C, Yin QW, Oppenheim RW: A novel type of programmed neuronal death in the cervical spinal cord of the chick embryo. J Neurosci 1996, 16:3685–3703
54. Ronnevi LO: Spontaneous phagocytosis of C-type synaptic terminals by spinal alpha-motoneurons in newborn kittens. An electron microscopic study. Brain Res 1979, 162:189–199
55. Borke RC: Perisomatic changes in the maturing hypoglossal nucleus after axon injury. J Neurocytol 1982, 11:463–485
56. Perry VH, O'Connor V: C1q: the perfect complement for a synaptic feast? Nat Rev Neurosci 2008, 9:807–811
57. Hogan RN, Baringer JR, Prusiner SB: Scrapie infection diminishes spines and increases varicosities of dendrites in hamsters: a quantitative Golgi analysis. J Neuropathol Exp Neurol 1987, 46:461–473
58. Brown D, Belichenko P, Sales J, Jeffrey M, Fraser JR: Early loss of dendritic spines in murine scrapie revealed by confocal analysis. Neuroreport 2001, 12:179–183
59. Chen Y, Dube CM, Rice CJ, Baram TZ: Rapid loss of dendritic spines after stress involves derangement of spine dynamics by corticotropin-releasing hormone. J Neurosci 2008, 28:2903–2911
60. Fifkova E, Delay RJ: Cytoplasmic actin in neuronal processes as a possible mediator of synaptic plasticity. J Cell Biol 1982, 95:345–350
61. Bourne JN, Harris KM: Balancing structure and function at hippocampal dendritic spines. Annu Rev Neurosci 2008, 31:47–67
62. Hering H, Sheng M: Dendritic spines: structure, dynamics and regulation. Nat Rev Neurosci 2001, 2:880–888
63. Star EN, Kwiatkowski DJ, Murthy VN: Rapid turnover of actin in dendritic spines and its regulation by activity. Nat Neurosci 2002, 5:239–246
64. Ackermann M, Matus A: Activity-induced targeting of profilin and stabilization of dendritic spine morphology. Nat Neurosci 2003, 6:1194–1200
65. Deng J, Dunaevsky A: Dynamics of dendritic spines and their afferent terminals: spines are more motile than presynaptic boutons. Dev Biol 2005, 277:366–377
66. Kaplan G: Differences in the mode of phagocytosis with Fc and C3 receptors in macrophages. Scand J Immunol 1977, 6:797–807
67. Betmouni S, Perry VH, Gordon JL: Evidence for an early inflammatory response in the central nervous system of mice with scrapie. Neuroscience 1996, 74:1–5
68. Jamieson E, Jeffrey M, Ironside JW, Fraser JR: Apoptosis and dendritic dysfunction precede prion protein accumulation in 87V scrapie. Neuroreport 2001, 12:2147–2153
69. Jeffrey M, Goodsir CM, Race RE, Chesebro B: Scrapie-specific neuronal lesions are independent of neuronal PrP expression. Ann Neurol 2004, 55:781–792